

CrystEngComm

Accepted Manuscript



This is an *Accepted Manuscript*, which has been through the Royal Society of Chemistry peer review process and has been accepted for publication.

Accepted Manuscripts are published online shortly after acceptance, before technical editing, formatting and proof reading. Using this free service, authors can make their results available to the community, in citable form, before we publish the edited article. We will replace this *Accepted Manuscript* with the edited and formatted *Advance Article* as soon as it is available.

You can find more information about *Accepted Manuscripts* in the [Information for Authors](#).

Please note that technical editing may introduce minor changes to the text and/or graphics, which may alter content. The journal's standard [Terms & Conditions](#) and the [Ethical guidelines](#) still apply. In no event shall the Royal Society of Chemistry be held responsible for any errors or omissions in this *Accepted Manuscript* or any consequences arising from the use of any information it contains.

Cite this: DOI: 10.1039/c0xx00000x

www.rsc.org/xxxxxx

ARTICLE TYPE

A New Strategy to Achieve $\text{La}_2\text{O}_2\text{CN}_2:\text{Eu}^{3+}$ Novel Luminescent One-dimensional Nanostructures

Xiaomin Guo, Jinxian Wang, Xiangting Dong*, Wensheng Yu and Guixia Liu

Received (in XXX, XXX) Xth XXXXXXXXXX 20XX, Accepted Xth XXXXXXXXXX 20XX

DOI: 10.1039/b000000x

$\text{La}_2\text{O}_3:\text{Eu}^{3+}$ nanofibers and nanobelts were fabricated by calcination of the respective electrospun PVP/[$\text{La}(\text{NO}_3)_3+\text{Eu}(\text{NO}_3)_3$] composite nanofibers and nanobelts. For the first time, $\text{La}_2\text{O}_2\text{CN}_2:\text{Eu}^{3+}$ nanofibers and nanobelts were successfully prepared via cyanamidation of $\text{La}_2\text{O}_3:\text{Eu}^{3+}$ respective nanostructures employing NH_3 gas and graphite at high temperature. X-ray powder diffraction (XRD) analysis indicates that $\text{La}_2\text{O}_2\text{CN}_2:\text{Eu}^{3+}$ nanostructures are tetragonal in structure with space group of $I4/mmm$. Scanning electron microscope (SEM) analysis reveals that the thickness and width of the $\text{La}_2\text{O}_2\text{CN}_2:\text{Eu}^{3+}$ nanobelts are respective ca. 192 nm and 1.67 ± 0.18 μm , and the diameters of $\text{La}_2\text{O}_2\text{CN}_2:\text{Eu}^{3+}$ nanofibers are 173.61 ± 21.61 nm under the 95% confidence level. Photoluminescence (PL) analysis manifests that the $\text{La}_2\text{O}_2\text{CN}_2:\text{Eu}^{3+}$ with different morphologies emits the predominant emission peaks at 614 nm and 622 nm originated from the energy levels transition ${}^5\text{D}_0\rightarrow{}^7\text{F}_2$ of Eu^{3+} ions under the excitation of 284-nm ultraviolet light. It is found that the optimum doping molar concentration of Eu^{3+} ions for $\text{La}_2\text{O}_2\text{CN}_2:\text{Eu}^{3+}$ nanostructures is 3%. $\text{La}_2\text{O}_2\text{CN}_2:\text{Eu}^{3+}$ nanofibers exhibit the stronger PL intensity than the nanobelts under the same doping concentration. CIE analysis demonstrates that color-tuned luminescence can be obtained by changing the concentration of doping activator ions and morphologies, which could be applied in the fields of optical telecommunication and optoelectronic devices. The possible formation mechanisms of $\text{La}_2\text{O}_2\text{CN}_2:\text{Eu}^{3+}$ nanofibers and nanobelts are also proposed. More importantly, the new strategy and construct technique are of universal significance to fabricate other rare earth oxycyanamide nanostructures with various morphologies.

1 Introduction

Recently, inorganic rare earth (RE) compounds containing several kinds of anions have been paid much attention as optical materials. Different kinds of anions can make their structure, physical and chemical properties unique and multiple. The structure of $(\text{REO})_n\text{X}$ is composed of alternating layers of the $(\text{REO})_n^{n+}$ complex cations and X^{n-} ($\text{X}=\text{S}, \text{Cl}, \text{Br}, \text{CO}_3, \text{SO}_4, \text{CN}_2$) anions^[1]. The $(\text{REO})_n^{n+}$ structural unit is very stable, which is assumed to be the reason for the exceptional luminescence properties of the RE oxycompounds^[2]. The exceptional luminescence and structural properties of the RE oxycompounds give an excellent opportunity to study the changes in the optical properties of a given RE^{3+} ion when the structure of the host is changed^[3-7]. Europium ions doped luminescent materials as the main and outstanding red emitting phosphors have attracted much attention of the scientists, and the ${}^5\text{D}_0\rightarrow{}^7\text{F}_J$ ($J=0-4$) transitions of Eu^{3+} ions result in important applications in displays^[8-10], lasers^[11,12], optical telecommunication^[13], and optoelectronic devices^[14]. More recently, their unique advantages have been envisaged in biosensing and medical diagnosis^[15-18].

Lanthanum oxycyanamide ($\text{La}_2\text{O}_2\text{CN}_2$) is the new luminescent matrix, which has potential applications in the fields of electroluminescent devices, polarizers and laser host materials. The luminescence properties of $\text{Ln}_2\text{O}_2\text{CN}_2:\text{RE}^{3+}$ ($\text{Ln}=\text{La}, \text{Y}$ and Gd ; $\text{RE}=\text{Pr}$ and Eu) have been reported^[2-4]. All the homologous $\text{Ln}_2\text{O}_2\text{CN}_2:\text{RE}^{3+}$ compounds were synthesized following the solid-state metathesis (SSM) method, and the morphologies of the products are only bulk particles. Presently, no reports on the preparation of $\text{La}_2\text{O}_2\text{CN}_2:\text{Eu}^{3+}$ nanofibers and nanoribbons are found in the literatures.

Nanofiber and nanobelt are new kinds of one-dimensional nanostructures with special morphologies. They have attracted

increasing interest of scientists owing to their anisotropy, large length-to-diameter ratio and width-to-thickness ratio, unique optical, electrical and magnetic performances^[19-28]. Research on the fabrication and properties of nanofibers and nanobelts has become one of the popular subjects of study in the realm of nanomaterials. Electrospinning is one technique that allows fabrication of continuous fibers with diameters ranging from tens of nanometers up to micrometers^[29]. It has been found that the electrospinning technology have already been applied in the fields of ultrafiltration, tissue engineering, catalysis, as well as devices that include solar cells, transistors, sensors, memories, etc^[29-36]. In this paper, Eu^{3+} doped $\text{La}_2\text{O}_2\text{CN}_2$ nanofibers and nanoribbons were successfully prepared by calcinating the electrospun PVP/[$\text{La}(\text{NO}_3)_3+\text{Eu}(\text{NO}_3)_3$] composites followed by cyanamidation, and the structure, morphology and PL properties of the resulting samples were investigated in detail. In addition, the formation mechanisms of $\text{La}_2\text{O}_2\text{CN}_2:\text{Eu}^{3+}$ nanostructures are also presented.

2 Experimental Sections

2.1 Chemicals

Polyvinyl pyrrolidone ($M_w=90000$, AR) were purchased from Tianjin Bodi Chemical Co. Ltd. N, N-dimethylformamide (DMF, AR) was bought from Tiantai Chemical Co. Ltd. La_2O_3 (99.99%) and Eu_2O_3 (99.99%) were supplied by China Pharmaceutical Group Shanghai Chemical Reagent Company. Nitric acid (HNO_3 , AR) was bought from Beijing chemical Co. Ltd. All chemicals were directly used as received without further purification.

2.2 Fabrication of $\text{La}_2\text{O}_2\text{CN}_2:x\%\text{Eu}^{3+}$ nanofibers

$\text{La}_2\text{O}_2\text{CN}_2:x\%\text{Eu}^{3+}$ [$x=1, 3, 5$, and 7 , x stands for molar

percentage of Eu^{3+} to $(\text{Eu}^{3+}+\text{La}^{3+})$ nanofibers were prepared by calcinating the electrospun PVP/[$\text{La}(\text{NO}_3)_3+\text{Eu}(\text{NO}_3)_3$] composites followed by cyanamidation. In the typical procedure of preparing representative $\text{La}_2\text{O}_2\text{CN}_2\cdot 3\%\text{Eu}^{3+}$ nanofibers, 0.9716 g of La_2O_3 and 0.0325 g of Eu_2O_3 were dissolved in dilute HNO_3 (1:1, volume ratio) at elevated temperature to form $\text{RE}(\text{NO}_3)_3\cdot 6\text{H}_2\text{O}$ powders ($\text{RE}=\text{La}^{3+}, \text{Eu}^{3+}$) by evaporating the excess HNO_3 and water from the solution by heating. The $\text{RE}(\text{NO}_3)_3\cdot 6\text{H}_2\text{O}$ powders were dissolved in 15.8 g of DMF. Then 2.2 g of PVP was added into the above solution under stirring for 4 h to form homogeneous transparent spinning solution. In the spinning solution, the mass ratio of PVP, rare earth nitrate and DMF is 11:10:79. Subsequently, the above spinning solution was loaded into a hypodermic syringe with a stainless steel needle (the inner diameter of the stainless steel needles is about 0.5 mm). The anode of the DC high power supply was connected to the needle tip of the syringe while the cathode was connected to the Fe net collector plate. The positive voltage applied to the tip was 13 kV and the solidification distance was 18 cm. The ambient temperature was 18–25 °C, and the relative humidity was 40%–60%. The flow rate of the spinning solution was determined by the contents of PVP in solutions because PVP can adjust the viscosity of solutions. PVP/[$\text{La}(\text{NO}_3)_3+\text{Eu}(\text{NO}_3)_3$] composite nanofibers were obtained on the collector with the evaporation of DMF. Then the above composite nanofibers were calcined at a rate of 1 °C/min and remained for 8 h at 700 °C. Thus, $\text{La}_2\text{O}_3\cdot 3\%\text{Eu}^{3+}$ nanofibers were obtained. The $\text{La}_2\text{O}_3\cdot 3\%\text{Eu}^{3+}$ nanofibers were loaded into a graphite boat-shaped crucible and then heated to 950 °C at the heating rate of 1 °C/min and remained for 12 h under a flow of gaseous ammonia. Then, the calcination temperature was decreased to 200 °C with a rate of 1 °C/min, followed by natural cooling down to room temperature, and $\text{La}_2\text{O}_2\text{CN}_2\cdot 3\%\text{Eu}^{3+}$ nanofibers were obtained. Other series of $\text{La}_2\text{O}_2\text{CN}_2\cdot x\%\text{Eu}^{3+}$ ($x=1, 5$ and 7) nanofibers were prepared by the similar procedures except for different doping molar concentration of Eu^{3+} ions.

2.3 Synthesis of $\text{La}_2\text{O}_2\text{CN}_2\cdot 3\%\text{Eu}^{3+}$ nanobelts

$\text{RE}(\text{NO}_3)_3\cdot 6\text{H}_2\text{O}$ ($\text{RE}=\text{La}^{3+}, \text{Eu}^{3+}$) powders were prepared by dissolving 0.9716 g of La_2O_3 and 0.0325 g of Eu_2O_3 in dilute HNO_3 (1:1, volume ratio) at elevated temperature. After evaporating, the obtained $\text{RE}(\text{NO}_3)_3\cdot 6\text{H}_2\text{O}$ powders were dissolved in 14.0 g of DMF. Then 4.0 g of PVP was added into the above solution under stirring for 12 h to form homogeneous transparent spinning solution. In this spinning solution, the mass ratio of PVP, rare earth nitrate and DMF is 20:10:70. The positive voltage applied to the tip was 8 kV and the solidification distance was 15 cm, and the other preparation conditions were the same as those for the nanofibers. Thus PVP/[$\text{La}(\text{NO}_3)_3+\text{Eu}(\text{NO}_3)_3$] composite nanobelts were obtained on the collector with the evaporation of DMF. Then the above composite nanobelts were calcined at a rate of 1 °C/min and remained for 8 h at 700 °C, and $\text{La}_2\text{O}_3\cdot 3\%\text{Eu}^{3+}$ nanobelts were obtained. $\text{La}_2\text{O}_2\text{CN}_2\cdot 3\%\text{Eu}^{3+}$ nanobelts were fabricated through cyanamidation of the obtained $\text{La}_2\text{O}_3\cdot 3\%\text{Eu}^{3+}$ nanobelts using the same process, as described in section 2.2. The variant preparation conditions for preparing the $\text{La}_2\text{O}_2\text{CN}_2\cdot 3\%\text{Eu}^{3+}$ nanofibers and nanobelts were listed in Table 1.

2.4 Characterization methods

X-ray diffraction (XRD) analysis was performed using a Rigaku D/max-RA XRD diffractometer with $\text{Cu K}\alpha$ radiation of 0.15406 nm. The size and morphology of the products were investigated by an XL-30 field emission scanning electron microscope (SEM) made by FEI Company. The purity of the products was examined

by OXFORD ISIS-300 energy dispersive X-ray spectrometer (EDX). The specific surface areas of the nanostructures were measured by a V-Sorb 2800P specific surface area and pore size analyzer made by Gold APP Instrument Corporation. The excitation and emission spectra of samples were recorded with a Hitachi F-7000 fluorescence spectrophotometer using a Xe lamp as the excitation source. In order to compare the PL intensity of the samples, all the determination conditions remain identical. All the measures were performed at room temperature.

Table 1 Preparation conditions of different nanostructures

| conditions | $\text{La}_2\text{O}_2\text{CN}_2\cdot 3\%\text{Eu}^{3+}$ nanofibers | $\text{La}_2\text{O}_2\text{CN}_2\cdot 3\%\text{Eu}^{3+}$ nanobelts |
|-----------------------------|--|---|
| PVP(g) | 2.2 | 4.0 |
| DMF(g) | 15.8 | 14.0 |
| Positive voltage(kV) | 13 | 8 |
| Solidification distance(cm) | 18 | 15 |

3 Results and discussion

3.1 XRD analysis

Fig. 1 shows the XRD patterns of the $\text{La}_2\text{O}_2\text{CN}_2\cdot \text{Eu}^{3+}$ nanofibers with different molar concentration of Eu^{3+} . As seen from Fig. 1, the characteristic diffraction peaks of all samples are observed in 2θ range of 10° – 90° , all of which can be readily indexed to those of the tetragonal crystal phase with primitive structure of $\text{La}_2\text{O}_2\text{CN}_2$ (PDF No. 83-0304), and the space group is $I4/mmm$. No other impurity phase can be detected at the current doping concentrations, indicating that the Eu^{3+} ions are completely inserted into the $\text{La}_2\text{O}_2\text{CN}_2$ host lattice through replacing the La^{3+} ions. However, the diffraction peaks of all samples are shifted to the higher diffraction angles compared with those of the $\text{La}_2\text{O}_2\text{CN}_2$ (PDF No. 83-0304), as shown in the insets of Fig. 1, 2, due to the different ionic radii between La^{3+} and Eu^{3+} , meaning that the lattice constants of $\text{La}_2\text{O}_2\text{CN}_2\cdot \text{Eu}^{3+}$ nanostructures have been slightly changed. The lattice constants are calculated using the following expression:

$$\sin^2\theta = (\lambda/2a)^2 \times (h^2 + k^2) + (\lambda/2c)^2 \times l^2$$

where λ value is 1.5406 Å, h , k and l are diffraction indexes, and the lattice constants of $\text{La}_2\text{O}_2\text{CN}_2\cdot \text{Eu}^{3+}$ nanofiber are $a=b=4.07$ Å and $c=12.21$ Å, respectively. The same structures are obtained for the $\text{La}_2\text{O}_2\text{CN}_2\cdot 3\%\text{Eu}^{3+}$ nanofiber and nanobelts, as manifested in Fig. 2.

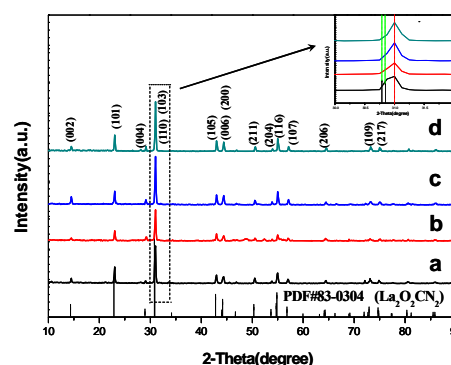


Fig. 1 XRD patterns of $\text{La}_2\text{O}_2\text{CN}_2\cdot x\%\text{Eu}^{3+}$ nanofibers [$x=1$ (a), 3 (b), 5 (c) and 7 (d)] with PDF standard card of $\text{La}_2\text{O}_2\text{CN}_2$

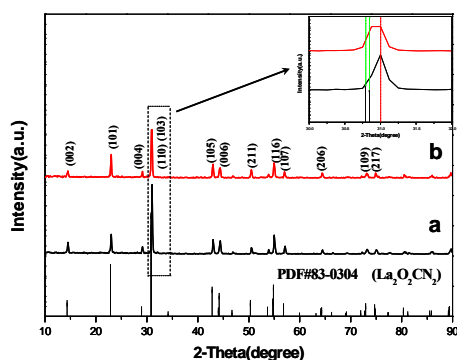


Fig. 2 XRD patterns of $\text{La}_2\text{O}_2\text{CN}_2:3\%\text{Eu}^{3+}$ nanobelts (a) and nanofibers (b) with PDF standard card of $\text{La}_2\text{O}_2\text{CN}_2$

3.2 Morphology observation

The morphologies of the products are characterized by scanning electron microscope (SEM). Fig. 3 demonstrates the representative SEM images of the composite nanofibers, composite nanobelts, $\text{La}_2\text{O}_2\text{CN}_2:3\%\text{Eu}^{3+}$ nanofibers and $\text{La}_2\text{O}_2\text{CN}_2:3\%\text{Eu}^{3+}$ nanobelts. From the SEM image of Fig. 3a, it can be noticed that the PVP/[$\text{La}(\text{NO}_3)_3+\text{Eu}(\text{NO}_3)_3$] composite nanofibers have smooth surface and uniform diameter. After annealing and cyanamidation at 950°C , the diameters of the nanofibers greatly decrease due to loss of the PVP and associated organic components, as-formed $\text{La}_2\text{O}_2\text{CN}_2:3\%\text{Eu}^{3+}$ nanofibers have relatively smooth surface and uniform diameter ranging from 120 nm to 230 nm, as revealed in Fig.3b. The SEM image of PVP/[$\text{La}(\text{NO}_3)_3+\text{Eu}(\text{NO}_3)_3$] composite nanobelts with the thickness of 230 nm (shown in the inset of Fig. 3c) is manifested in Fig. 3c, the composite nanobelts are smooth and uniform. Clearly, uniform $\text{La}_2\text{O}_2\text{CN}_2:3\%\text{Eu}^{3+}$ nanobelts with the thickness of 192 nm are synthesized and have relatively smooth surface, as indicated in Fig. 3d. Preliminarily, we can conclude that the cyanamidation process can retain the morphologies of the nanofibers and nanobelts used as precursors.

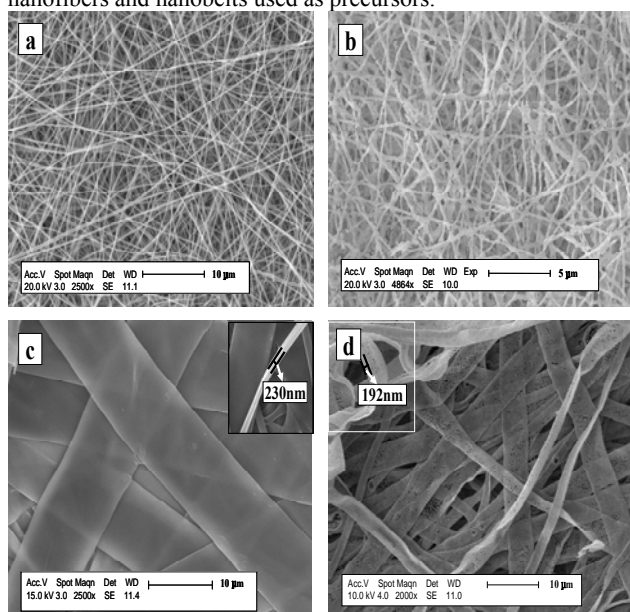


Fig. 3 SEM images of PVP/[$\text{La}(\text{NO}_3)_3+\text{Eu}(\text{NO}_3)_3$] composite nanofibers (a), $\text{La}_2\text{O}_2\text{CN}_2:3\%\text{Eu}^{3+}$ nanofibers (b), PVP/[$\text{La}(\text{NO}_3)_3+\text{Eu}(\text{NO}_3)_3$] composite nanobelts (c) and $\text{La}_2\text{O}_2\text{CN}_2:3\%\text{Eu}^{3+}$ nanobelts (d)

Under the 95% confidence level, the diameters of composite nanofibers and $\text{La}_2\text{O}_2\text{CN}_2:3\%\text{Eu}^{3+}$ nanofibers, the widths of

composite nanobelts and $\text{La}_2\text{O}_2\text{CN}_2:3\%\text{Eu}^{3+}$ nanobelts analyzed by Shapiro–Wilk method are normal distribution. Distribution histograms of diameters and widths of the nanostructures are indicated in Fig. 4. As seen from Fig. 4, the diameters of composite nanofibers and as-formed $\text{La}_2\text{O}_2\text{CN}_2:3\%\text{Eu}^{3+}$ nanofibers, the widths of composite nanobelts and $\text{La}_2\text{O}_2\text{CN}_2:3\%\text{Eu}^{3+}$ nanobelts are 210.14 ± 15.08 nm, 173.61 ± 21.61 nm, 10.82 ± 0.38 μm and 1.67 ± 0.18 μm , respectively.

The elementary compositions of $\text{La}_2\text{O}_2\text{CN}_2:3\%\text{Eu}^{3+}$ nanofibers and $\text{La}_2\text{O}_2\text{CN}_2:3\%\text{Eu}^{3+}$ nanobelts are further confirmed by energy dispersive X-ray spectrometer (EDX), as reveals in Fig.5. The energy dispersive spectra reveal the presence of La, Eu, O, C and N elements in $\text{La}_2\text{O}_2\text{CN}_2:3\%\text{Eu}^{3+}$ nanofibers and nanobelts. The element of Au in the spectra comes from the Au film coated on the surface of the sample for SEM observation. No other elements are found in the samples, indicating that the $\text{La}_2\text{O}_2\text{CN}_2:3\%\text{Eu}^{3+}$ nanostructures are highly pure.

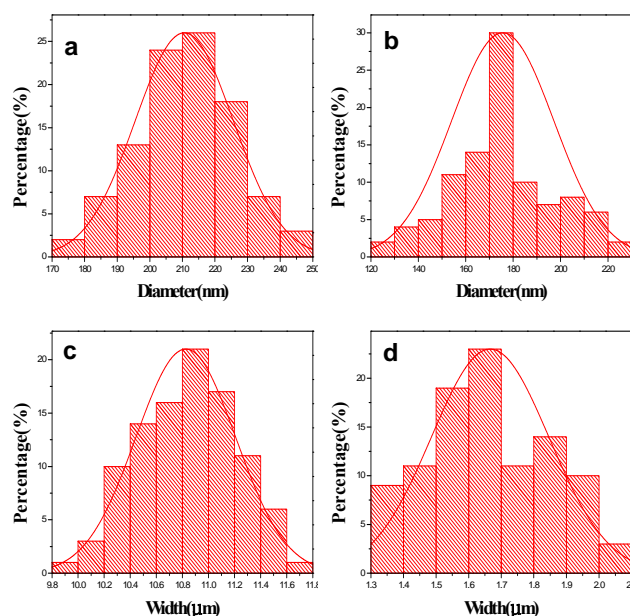


Fig. 4 Distribution histograms of the diameters of PVP/[$\text{La}(\text{NO}_3)_3+\text{Eu}(\text{NO}_3)_3$] composite nanofibers (a), $\text{La}_2\text{O}_2\text{CN}_2:3\%\text{Eu}^{3+}$ nanofibers (b) and the widths of PVP/[$\text{La}(\text{NO}_3)_3+\text{Eu}(\text{NO}_3)_3$] composite nanobelts (c) and $\text{La}_2\text{O}_2\text{CN}_2:3\%\text{Eu}^{3+}$ nanobelts (d)

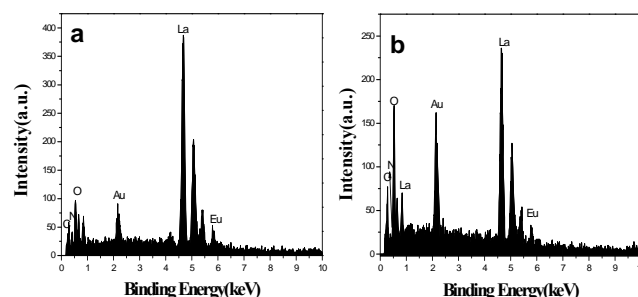


Fig. 5 EDX images of $\text{La}_2\text{O}_2\text{CN}_2:3\%\text{Eu}^{3+}$ nanofibers (a) and nanobelts (b)

3.3 BET analysis

The specific surface areas of the $\text{La}_2\text{O}_2\text{CN}_2:3\%\text{Eu}^{3+}$ nanofibers and nanobelts are determined by BET method. The measured BET surface area adsorption isotherms of $\text{La}_2\text{O}_2\text{CN}_2:3\%\text{Eu}^{3+}$ nanostructures are shown in Fig.6. The adsorption saturation capacity of nanofibers and nanobelts, which are obtained

respectively from the Fig. 6, are 3.45 mL, 3.15 mL, respectively. The BET model surface areas are calculated using the following formula:

$$\text{BET} = [(V_m \times 10^{-3}) / 22.4] \times 6.02 \times 10^{23} \times 1.62 \times 10^{-19}$$

where V_m is the adsorption saturation capacity, and the BET model surface areas of nanofibers and nanobelts are calculated to be $15.0 \text{ m}^2 \cdot \text{g}^{-1}$ and $13.7 \text{ m}^2 \cdot \text{g}^{-1}$, respectively. Remarkably, the specific surface area of $\text{La}_2\text{O}_2\text{CN}_2:3\%\text{Eu}^{3+}$ nanofibers is bigger than that of $\text{La}_2\text{O}_2\text{CN}_2:3\%\text{Eu}^{3+}$ nanobelts.

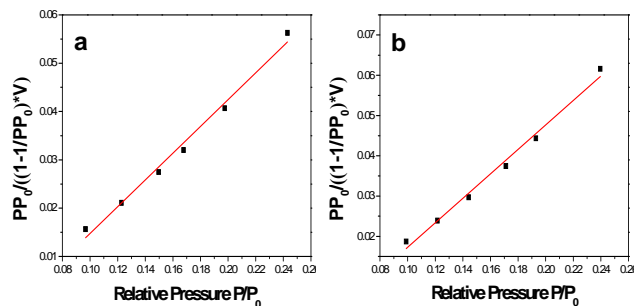


Fig. 6 BET surface area adsorption isotherms of $\text{La}_2\text{O}_2\text{CN}_2:3\%\text{Eu}^{3+}$ nanofibers (a) and nanobelts (b)

3.4 Photoluminescence properties

Fig.7 illustrates the excitation (monitored by 622 nm) and emission (excited by 284 nm) spectra of the $\text{La}_2\text{O}_2\text{CN}_2:3\%\text{Eu}^{3+}$ nanofibers. The excitation spectrum (Fig. 7a) exhibits one broad band in the range from 250 to 350 nm. The predominant peak at 284 nm is associated with the charge-transfer band (CTB) of $\text{Eu}^{3+}-\text{O}^{2-}$, the CTB of $\text{La}_2\text{O}_2\text{CN}_2:3\%\text{Eu}^{3+}$ corresponds to the electron transition from the 2p orbital of O^{2-} to the 4f orbital of Eu^{3+} . In the longer wavelength region, the characteristic f-f transition peaks (at 367 nm, ${}^7\text{F}_0 \rightarrow {}^5\text{D}_4$; 383 nm, ${}^7\text{F}_0 \rightarrow {}^5\text{G}_2$; 395 nm, ${}^7\text{F}_0 \rightarrow {}^5\text{L}_6$; 417 nm, ${}^7\text{F}_0 \rightarrow {}^5\text{D}_3$; 468 nm, ${}^7\text{F}_0 \rightarrow {}^5\text{D}_2$) of Eu^{3+} ions can be observed with very weak intensity compared with that of the CTB^[19].

The emission (excited by 284 nm) spectrum of $\text{La}_2\text{O}_2\text{CN}_2:3\%\text{Eu}^{3+}$ nanofibers is shown in the Fig.7b. The luminescence from the ${}^5\text{D}_0$ level of the Eu^{3+} ion is found to be efficient, whereas emission from the higher excited states ${}^5\text{D}_1, 2$ is quenched due to the multi-phonon processes. The spectrum is characterized by an intense, characteristic red emission of predominant peaks which splits into two peaks at 614 nm and 622 nm originating from the transition along with dominating electric dipole transitions ${}^5\text{D}_0 \rightarrow {}^7\text{F}_2$ of Eu^{3+} , indicating that Eu^{3+} occupies a site with no inversion center low symmetries in the $\text{La}_2\text{O}_2\text{CN}_2:\text{Eu}^{3+}$ nanofibers. The magnetic dipole transitions ${}^5\text{D}_0 \rightarrow {}^7\text{F}_0$, ${}^5\text{D}_0 \rightarrow {}^7\text{F}_1$ and especially ${}^5\text{D}_0 \rightarrow {}^7\text{F}_3$ are weak^[3]. These transitions are hypersensitive to crystal-structure and chemical surroundings^[37,38].

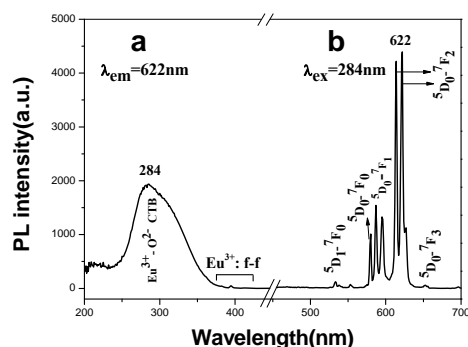


Fig. 7 Excitation (a) and Emission (b) spectra of the $\text{La}_2\text{O}_2\text{CN}_2:3\%\text{Eu}^{3+}$ nanofibers

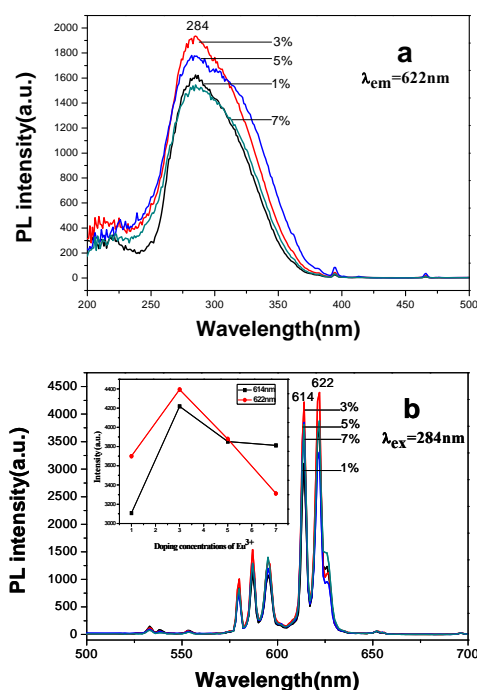


Fig. 8 Excitation (a) and Emission (b) spectra of $\text{La}_2\text{O}_2\text{CN}_2:\text{Eu}^{3+}$ nanofibers doped with various concentrations of Eu^{3+} ions. The inset is the dependence of its PL intensity on the Eu^{3+} content in the $\text{La}_2\text{O}_2\text{CN}_2$ matrix

Fig.8 demonstrates the PL spectra of $\text{La}_2\text{O}_2\text{CN}_2:\text{Eu}^{3+}$ nanofibers with different doping concentrations of Eu^{3+} ions. It is found that the spectral shape and locations of excitation and emission peaks do not vary with the doping concentrations of Eu^{3+} ions for $\text{La}_2\text{O}_2\text{CN}_2:\text{Eu}^{3+}$ nanofibers, but the intensity of excitation and emission peaks for $\text{La}_2\text{O}_2\text{CN}_2:x\%\text{Eu}^{3+}$ nanofibers strongly depend on the doping concentration of Eu^{3+} ions, and the strongest excitation and emission spectra can be obtained when the doping molar concentration of Eu^{3+} is 3%. Obviously, the luminescence intensity of $\text{La}_2\text{O}_2\text{CN}_2:\text{Eu}^{3+}$ nanofibers increases with the increase of the concentration of Eu^{3+} from the beginning, reaches a maximum value with the Eu^{3+} concentration of 3%, and then decreases with further increase in Eu^{3+} concentration. While considering the mechanism of energy transfer in phosphors, the concentration quenching can be explained in more detail by critical distance (R_c), and the critical distance (R_c) between Eu^{3+} ions for energy transfer can be calculated using the formula that was proposed by Blasse and Grabmaier as below^[39]:

$$R_c = 2 \times (3V/4\pi X_c N)^{1/3}$$

where V is the volume of the unit cell, X_c is the critical concentration of activator ions and N is the number of formula unit per unit cell. In case of $\text{La}_2\text{O}_2\text{CN}_2:3\%\text{Eu}^{3+}$ nanofibers, $X_c=0.03$, $V=0.2022 \text{ nm}^3$ and $N=4$. Therefore, the average distances R_c between Eu^{3+} ions is calculated to be $R_c=1.4766 \text{ nm}$ when the doping optimum molar concentration is 3%.

PL decay curves of $\text{La}_2\text{O}_2\text{CN}_2:x\%\text{Eu}^{3+}$ nanofibers with different concentration of Eu^{3+} (1, 3, 5, and 7%) are shown in Fig.9. The samples are excited by 284 nm and monitored at 622 nm. It can be seen that all the curves can be well-fitted into a double-exponential function as $I = A_1 \exp(-t/s_1) + A_2 \exp(-t/s_2)$, in which s_1 and s_2 are the fast and slow components of the luminescence lifetimes, A_1 and A_2 are the fitting parameters. It indicates that the average lifetime of $\text{La}_2\text{O}_2\text{CN}_2:x\%\text{Eu}^{3+}$ nanofibers [$x=1, 3, 5$ and 7] are 0.869 ms, 1.023 ms, 0.923 ms and 0.887 ms, respectively.

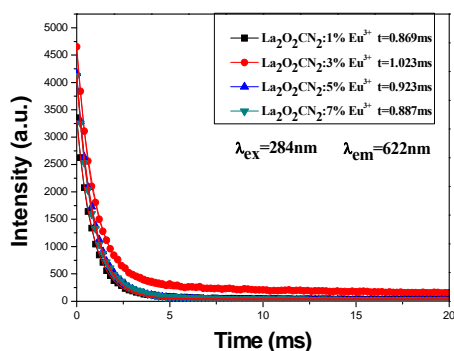


Fig. 9 Luminescence decay curves of $\text{La}_2\text{O}_2\text{CN}_2:\text{Eu}^{3+}$ nanofibers doped with various concentrations of Eu^{3+} ions

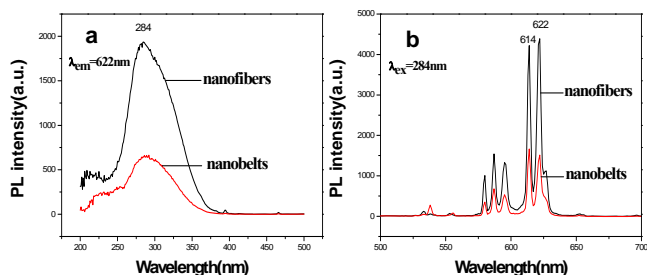


Fig. 10 Excitation (a) and Emission (b) spectra of $\text{La}_2\text{O}_2\text{CN}_2:3\%\text{Eu}^{3+}$ nanofibers and nanobelts

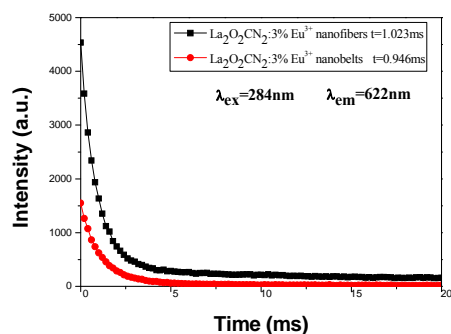


Fig. 11 Luminescence decay curves of $\text{La}_2\text{O}_2\text{CN}_2:3\%\text{Eu}^{3+}$ nanofibers and nanobelts

Fig.10 demonstrates the comparison between the excitation and emission spectra of the $\text{La}_2\text{O}_2\text{CN}_2:3\%\text{Eu}^{3+}$ nanofibers and nanobelts measured under the same conditions. It can be found that the nanofibers have higher PL intensity than that of nanobelts. From above BET analysis, it is found that the specific surface area of the $\text{La}_2\text{O}_2\text{CN}_2:3\%\text{Eu}^{3+}$ nanofibers and nanobelts determined by BET method are $15.0 \text{ m}^2\cdot\text{g}^{-1}$ and $13.7 \text{ m}^2\cdot\text{g}^{-1}$, respectively. Remarkably, the specific surface area of the nanofibers is bigger than that of the nanobelts, implying that the nanofibers have more surface luminescence centers than the nanobelts, as a result, the nanofibers have stronger luminescence than the nanobelts. Similar results were observed in the references^[22,23].

Fig.11 depicts the luminescence decay curves of $\text{La}_2\text{O}_2\text{CN}_2:3\%\text{Eu}^{3+}$ with different morphologies excited by 284 nm and monitored at 622 nm. The curves also can be well-fitted into a double-exponential function and the fitted lifetime is $\tau=1.023 \text{ ms}$ for the $\text{La}_2\text{O}_2\text{CN}_2:3\%\text{Eu}^{3+}$ nanofibers higher than that (0.946 ms) for the $\text{La}_2\text{O}_2\text{CN}_2:3\%\text{Eu}^{3+}$ nanobelts. The results reveal that the fluorescence lifetime is direct proportion to the luminescence intensity.

3.5 CIE analysis

In general, color can be represented by the Commission

Internationale de L'Eclairage (CIE) 1931 chromaticity coordinates. Fig.12a shows the chromaticity coordinates of $\text{La}_2\text{O}_2\text{CN}_2:x\%\text{Eu}^{3+}$ [$x=1, 3, 5$ and 7] nanofibers, and the chromaticity coordinates are respectively determined to be [(0.612, 0.354), (0.617, 0.355), (0.601, 0.349), (0.625, 0.352)]. The chromaticity coordinates of $\text{La}_2\text{O}_2\text{CN}_2:3\%\text{Eu}^{3+}$ nanofibers (0.617, 0.355) and nanobelts (0.577, 0.359) are represented in Fig.12b. These results indicate that the color emissions can be tuned by changing the concentration of doping activator ions and the morphologies of nanostructures. These nanostructures could show merits of red emissions, which are considered to be promising candidates for application in LEDs.

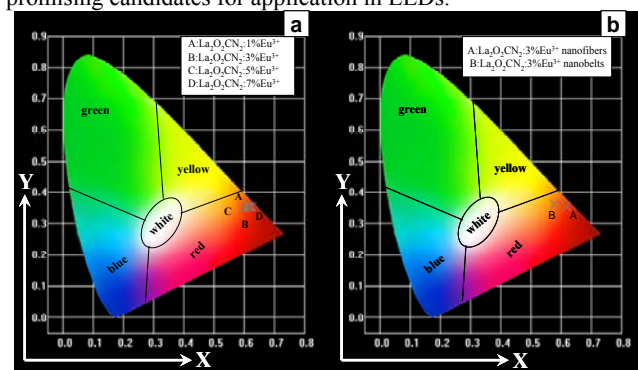
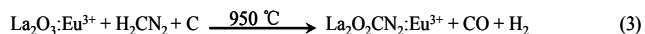
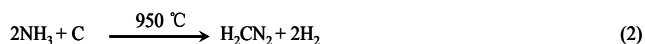
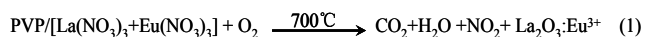


Fig. 12 CIE chromaticity coordinates diagram of $\text{La}_2\text{O}_2\text{CN}_2:x\%\text{Eu}^{3+}$ ($x=1, 3, 5, 7$) nanofibers(a) and $\text{La}_2\text{O}_2\text{CN}_2:3\%\text{Eu}^{3+}$ nanostructures(b)

3.6 Formation mechanisms for the $\text{La}_2\text{O}_2\text{CN}_2:\text{Eu}^{3+}$ nanostructures

According to the above analysis, we advance the formation mechanisms of $\text{La}_2\text{O}_2\text{CN}_2:\text{Eu}^{3+}$ nanostructures, as shown in Fig. 13. PVP, $\text{Eu}(\text{NO}_3)_3$ and $\text{La}(\text{NO}_3)_3$ were mixed with DMF to form spinning solution. PVP acted as template during the formation of $\text{La}_2\text{O}_2\text{CN}_2:\text{Eu}^{3+}$ nanostructures. La^{3+} , Eu^{3+} and NO_3^- were mixed or absorbed onto PVP to form $\text{PVP}/[\text{La}(\text{NO}_3)_3+\text{Eu}(\text{NO}_3)_3]$ composite nanofibers and nanobelts via electrospinning. Because the viscosity of the spinning solution for fabricating nanofibers was lower, and the applied voltage was higher, the spinning velocity was faster. The charge repulsion force acted on the radial direction of the jets had not enough time to stretch the jets into belt shape, resulted in the formation of composite nanofibers. Whereas the viscosity of the spinning solution for preparing nanobelts was higher, and the applied voltage was lower, so that the spinning velocity was slower. The charge repulsion force had adequate time to stretch the jets into belt shape, led to the formation of composite nanobelts. The morphologies of the composite nanostructures were basically retained after performing the following calcination and cyanamidation process. During calcination process, PVP was decomposed soon and carbonized, as well as nitrates were decomposed and oxidized to produce NO_2 , and eventually evaporated from the composite fibers and belts. With the increase in the calcining temperature, La^{3+} and Eu^{3+} ions could combine with O_2 , coming from air, to form $\text{La}_2\text{O}_3:\text{Eu}^{3+}$ crystallite, and many crystallites were combined into nanoparticles, and finally these nanoparticles were mutually connected to generate $\text{La}_2\text{O}_3:\text{Eu}^{3+}$ nanofibers and nanobelts. Afterwards, the above products were cyanamidated in a graphite boat under the flowing NH_3 . In the cyanamidation process, the carbon from graphite boat reacts with the flowing ammonia gas to produce H_2CN_2 and H_2 , then the as-prepared $\text{La}_2\text{O}_3:\text{Eu}^{3+}$ reacts with H_2CN_2 and graphite to produce $\text{La}_2\text{O}_2\text{CN}_2:\text{Eu}^{3+}$, CO and H_2 in the high temperature. During the process, graphite boat is not only a container, but also a reactant substance through reacting with NH_3 and $\text{La}_2\text{O}_3:\text{Eu}^{3+}$ in

the heating process. Reaction schemes for formation of $\text{La}_2\text{O}_2\text{CN}_2:\text{Eu}^{3+}$ nanostructures proceed as follows:



If the $\text{La}_2\text{O}_3:\text{Eu}^{3+}$ nanofibers were cyanamidated in a traditional corundum boat-shaped crucible (S1) or in a traditional corundum boat-shaped crucible loaded with some carbon rods (S2) under the flowing NH_3 in the same heating process, $\text{La}_2\text{O}_2\text{CN}_2:\text{Eu}^{3+}$ can not be obtained except $\text{La}_2\text{O}_3:\text{Eu}^{3+}$, which is confirmed by XRD patterns of the product, as indicated in Fig. 14. On the other hand, if $\text{La}_2\text{O}_3:\text{Eu}^{3+}$ nanofibers or nanobelts directly mix with the liquid H_2CN_2 , the H_2CN_2 will cut the $\text{La}_2\text{O}_3:\text{Eu}^{3+}$ nanofibers or nanobelts into pieces when heating. Cyanamidation technology we proposed here is actually a solid-gas reaction, which has been proved to be an important method, not only can retain the morphology of precursor, but also can fabricate pure phase $\text{La}_2\text{O}_2\text{CN}_2:\text{Eu}^{3+}$ nanostructures.

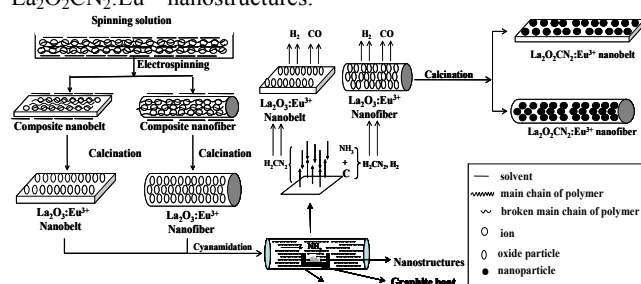


Fig. 13 Schematic diagram of formation mechanisms of $\text{La}_2\text{O}_2\text{CN}_2:\text{Eu}^{3+}$ nanofiber and nanobelt

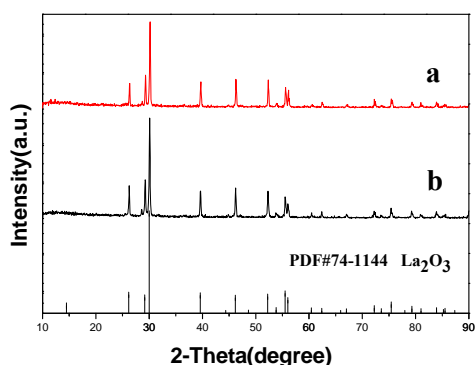


Fig. 14 XRD patterns of the products cyanamidated in processes S1 (a) and S2 (b) with PDF standard card of La_2O_3

4 Conclusions

In summary, pure tetragonal phase $\text{La}_2\text{O}_2\text{CN}_2:\text{Eu}^{3+}$ nanofibers and nanobelts with space group of $I4/mmm$ have been successfully prepared. The as-prepared $\text{La}_2\text{O}_2\text{CN}_2:\text{Eu}^{3+}$ nanostructures have relatively smooth surface, the diameter of the nanofibers is $173.61 \pm 21.61 \text{ nm}$, and the width of the nanobelts is $1.67 \pm 0.18 \mu\text{m}$. Under the excitation of 284-nm ultraviolet light, $\text{La}_2\text{O}_2\text{CN}_2:\text{Eu}^{3+}$ nanostructures exhibit the characteristic red emission of predominant peak which splits into two peaks at 614 and 622 nm originated from the energy levels transition ${}^5\text{D}_0 \rightarrow {}^7\text{F}_2$ of Eu^{3+} , indicating that Eu^{3+} occupies a site without inversion symmetry in the $\text{La}_2\text{O}_2\text{CN}_2:\text{Eu}^{3+}$ nanostructures. The strongest luminescence of $\text{La}_2\text{O}_2\text{CN}_2:x\% \text{Eu}^{3+}$ nanofibers is obtained when doping concentration of Eu^{3+} is 3%. The nanofibers have the stronger photoluminescence than the nanobelts under the same

measuring conditions. Color-tuned luminescence of $\text{La}_2\text{O}_2\text{CN}_2:\text{Eu}^{3+}$ nanostructures can be obtained by changing the doping concentration of Eu^{3+} and the morphologies of nanostructures. The new strategy and construct technique are of universal significance to fabricate other earth oxycyanamide nanostructures with various morphologies.

Acknowledgments

This work was financially supported by the National Natural Science Foundation of China (NSFC 50972020, 51072026), Ph.D. Programs Foundation of the Ministry of Education of China (20102216110002, 20112216120003), the Science and Technology Development Planning Project of Jilin Province (Grant Nos. 20130101001JC, 20070402, 20060504), the Research Project of Science and Technology of Department of Education of Jilin Province "11th 5-year plan" (Grant Nos. 2010JYT01), Key Research Project of Science and Technology of Ministry of Education of China (Grant No. 207026).

Notes and references

Key Laboratory of Applied Chemistry and Nanotechnology at Universities of Jilin Province, Changchun University of Science and Technology, Changchun 130022. Fax: 86 0431 85383815; Tel: 86 0431 85582574; E-mail: dongxiangting888@163.com

- T. Takeda, N. Hatta and S. Kikkawa. *Chem. Lett.*, 2006, **35**, 988-989.
- J. Hölsä, R.-J. Lamminmäki, M. Lastusaari, E. Säilynoja, P. Porcher, P. Dereñ and W. Stręk. *Spectrochim. Acta. Part A*, 1998, **54**, 2065-2069.
- E. Säilynoja, M. Lastusaari, J. Hölsä and P. Porcher. *J. Lumin.*, 1997, **72-74**, 201-203.
- J. Hölsä, R.-J. Lamminmäki, M. Lastusaari, P. Porcher and E. Säilynoja. *J. Alloys. Compd.*, 1998, **275-277**, 402-406.
- J. Sindlinger, J. Glaser, H. Bettentrup, T. Jüstel und H.-J. Meyer, *Z. Anorg. Allg. Chem.*, 2007, **633**, 1686-1690.
- Shunhao Pan, Ruiping Deng, Jing Feng, Shuyan Song, Song Wang, Min Zhu and Hongjie Zhang. *CrystEngComm*, 2013, **15**, 7640-7643.
- Yuhua Zheng, Hongpeng You, Guang Jia, Kai Liu, Yanhua Song, Mei Yang and Hongjie Zhang. *Cryst. Growth Des.*, 2009, **9**, 5101-5107.
- Y. S. Liu, D. T. Tu, H. M. Zhu, R. F. Li, W. Q. Luo and X. Y. Chen. *Adv. Mater.*, 2010, **22**, 3266-3271.
- Q. B. Li, J. M. Lin, J. H. Wu, L. Zhang, J. L. Wang, Y. Wang, F. G. Peng, M. L. Huang and Y. M. Xiao. *Chin. Sci. Bull.*, 2011, **56**, 3114-3118.
- H. Wang, C. K. Lin, X. M. Liu and J. Lin, *Appl. Phys. Lett.*, 2005, **87**, 181907-181907-3.
- J. R. O. Connor, *Appl. Phys. Lett.*, 1966, **9**, 407-409.
- V. I. Klimov, A. A. Mikhailovsky, S. Xu, A. Malko, J. A. Hollingsworth, C. A. Leatherdale, H. J. Eisler and M. G. Bawendi. *Science*, 2000, **290**, 314-317.
- D. B. Barber, C. R. Pollock, L. L. Beecroft and C. K. Ober. *Opt. Lett.*, 1997, **22**, 1247-1249.
- J. C. Heikenfeld, D.-S. Lee, M. J. Garter, C. C. Baker, Y. Q. Wang and R. Jones. *IEEE J. Sel. Top. Quant.*, 2002, **8**, 749-766.
- G. S. Yi, H. C. Lu, S. Y. Zhao, Y. Ge, W. J. Yang, D. P. Chen and L.-H. Guo. *Nano. Lett.*, 2004, **4**, 2191-2196.
- F. Meiser, C. Cortez and F. Caruso. *Angew. Chem. Int. Ed.*, 2004, **43**, 5954-5957.
- S. L. Yuan, Y. X. Yang, F. Chevre, F. Tessier, X. H. Zhang and G. R. Chen. *J. Am. Ceram. Soc.*, 2010, **93**, 3052-3055.
- Song Wang, Jing Feng, Shuyan Song and Hongjie Zhang. *CrystEngComm*, 2013, **15**, 7142-7151.
- L. Y. Yang, J. X. Wang, X. T. Dong, G. X. Liu and W. S. Yu. *J. Mater. Sci.*, 2013, **48**, 644-650.
- D. Li, W. S. Yu, X. T. Dong, J. X. Wang and G. X. Liu. *J. Fluorine Chem.*, 2013, **145**, 70-76.
- D. Li, X. T. Dong, W. S. Yu, J. X. Wang and G. X. Liu. *J. Mater. Sci.*, 2013, **24**, 3041-3048.

- 22 W. W. Ma, X. T. Dong, J. X. Wang, W. S. Yu and G. X. Liu. *J. Mater. Sci.*, 2013, **48**, 2557-2565.
- 23 Q. L. Kong, J. X. Wang, X. T. Dong, W. S. Yu and G. X. Liu. *J. Mater. Sci-Mater. Electron.*, 2013, **24**, 4745-4756.
- 24 Q. L. Ma, W. S. Yu, X. T. Dong, J. X. Wang, G. X. Liu and J. Xu. *Opt. Mater.*, 2013, **35**, 526-530.
- 25 Q. L. Ma, W. S. Yu, X. T. Dong, J. X. Wang, G. X. Liu and J. Xu. *J. Nanopart. Res.*, 2012, **14**, 1203-1209.
- 26 Q. L. Ma, J. X. Wang, X. T. Dong, W. S. Yu and G. X. Liu. *Chem. Eng. J.*, 2013, **222**, 16-22.
- 27 Q. L. Ma, J. X. Wang, X. T. Dong, W. S. Yu and G. X. Liu. *ChemPlusChem*, 2013, DOI: 10.1002/cplu.201300262.
- 28 Q. L. Ma, W. S. Yu, X. T. Dong, J. X. Wang and G. X. Liu, *Nanoscale*, 2013, DOI:10.1039/C3NR05472A.
- 29 A. Greiner, J. H. Wendorff. *Angew. Chem. Int. Ed.*, 2007, **46**, 5670-5703.
- 30 Yuechen Chou, Changlu Shao, Xinghua Li, Chunyan Su, Hongchuan Xu, Mingyi Zhang, Peng Zhang, Xin Zhang, Yichun Liu. *Appl. Surf. Sci.*, 2013, **285**, 509-516.
- 31 F. S. Kim, G. Q. Ren and S. A. Jenekhe. *Chem. Mater.*, 2011, **23**, 682-732.
- 32 N. Bhardwaj and S. C. Kundu. *Biotechnol. Adv.*, 2010, **28**, 325-347.
- 33 S. Chen, H. Hou, F. Harnisch, S. A. Patil, A. A. Carmona-Martinez, S. Agarwal, Y. Zhang, S.-R. Suman, L. Y. Alexander, A. Greiner and U. Schröder, *Energy Environ. Sci.*, 2011, **4**, 1417-1421.
- 34 C. J. Luo, S. D. Stoyanov, E. Stride, E. Pelan and M. Edirisinghe. *Chem. Soc. Rev.*, 2012, **41**, 4708-4735.
- 35 K. Garg, G. L. Bowlin. *Biomicrofluidics*, 2011, **5**, 013403-1-013403-19.
- 36 J.-P. Chen, Y.-S. Chang. *Colloids. Surf., B: Biointerfaces*. 2011, **86**, 169-175.
- 37 T. M. Chou, S. Mylswamy, R. S. Liu and S. Z. Chuang, *Solid. State. Commun.*, 2005, **136**, 205-209.
- 38 J. Thirumalai, R. Chandramohan, R. Divakar, E. Mohandas, M. Sekar and P. Parameswaran. *Nanotechnology*, 2008, **19**, 455-458.
- 39 G. Blasse. *Phys. Lett. A*, 1968, **28**, 444-445.